Predictability of landslide timing from quasi-periodic precursory earthquakes

Predictability of landslide timing from quasi-periodic precursory earthquakes

Andrew F. Bell [1]

[1]School of GeoSciences, University of Edinburgh, Edinburgh, U.K.

Corresponding author: Andrew Bell (a.bell@ed.ac.uk)

Key Points:

- A large landslide in Greenland was preceded by a rapid power-law acceleration in earthquake rates, faster than existing models predict
- Earthquake characteristics indicate repeated quasi-periodic activation of single source, driven by accelerated loading
- New Bayesian gamma point process method successfully used to model earthquakes and offer improved probabilistic forecasts of future landslides

Abstract

Accelerating rates of geophysical signals are observed before a range of material failure phenomena. They provide insights into the physical processes controlling failure and the basis for failure forecasts. However, examples of accelerating seismicity before landslides are rare, and their behavior and forecasting potential are largely unknown. Here I use a Bayesian methodology to apply a novel gamma point process model to investigate a sequence of quasi-periodic repeating earthquakes preceding a large landslide at Nuugaatsiaq in Greenland in June 2017. The evolution in earthquake rate is best explained by an inverse power-law increase with time towards failure, as predicted by material failure theory. However, the commonly accepted power-law exponent value of 1.0 is inconsistent with the data. Instead, the mean posterior value of 0.71 indicates a particularly rapid acceleration towards failure, and suggests only relatively short warning times may be possible for similar landslides in future.

1. Introduction

Accelerating rates of seismicity and ground deformation have been reported before a variety landslides (Amitrano et al., 2005; Caplan-Auerbach & Huggel, 2007; Intrieri et al., 2017; Kilburn & Petley, 2003; Petley et al., 2005; Poli, 2017) as well as other natural failure phenomena including volcanic eruptions (Dmitrieva et al., 2013; De La Cruz-Reyna & Reyes-Dávila, 2001; Minakami T., 1960; Omori, 1916; Salvage & Neuberg, 2016; Tokarev, 1963; Voight, 1988), and earthquakes (Bouchon et al., 2011; Peng et al., 2007). The apparent repetition of similar signals across these different types of systems suggest that the underlying processes all obey similar statistical physics. Similarities between reported accelerating trends in the Earth and those associated with material failure phenomena in the laboratory (Main, 1999; Vasseur et al., 2017) mean that they are often analysed within this conceptual framework (Kilburn & Petley, 2003; Main, 1999; Voight, 1988). Progressive material failure (in response to elevated stress) can often be approximated by an empirical relation which describes the acceleration in a geophysical precursor Ω (such as strain or number of earthquakes) as a function of its rate by:

$$\frac{d^2\Omega}{dt^2} = K\left(\frac{d\Omega}{dt}\right)^{\alpha} \quad (1)$$

where α and K are constants (Voight, 1988). Equation (1) is commonly known as the Failure Forecast Method (FFM). For different values of α, the expected evolution of precursor rate with time takes different forms. In the general case that $1 < \alpha < 2$ solutions to Equation (1) take the form of an inverse power-law increase in the mean rate of precursory signals with time (Kilburn, 2003):

$$\frac{d\Omega}{dt} = k_{pl}\left(t_f - t\right)^{-p} \quad (2)$$

where the power-law exponent, $p = 1/(\alpha - 1)$ describes the non-linearity of the acceleration, and k_{pl} is the absolute rate at $t = t_f - 1$ (Bell & Kilburn, 2013). For the specific cases of $\alpha = 1$ and $\alpha = 2$, respectively, the acceleration takes the form of either an exponential:

$$\frac{d\Omega}{dt} = k_e e^{\lambda(t-t_0)} \quad (3)$$

or hyperbolic:

$$\frac{d\Omega}{dt} = k_{hyp}\left(t_f - t\right)^{-1} \quad (4)$$

increase in rate with time, with corresponding amplitude terms k_e and k_{hyp}, and where t_0 corresponds to the time of the start of the failure process. Equations (2) & (4) involve a

singularity at a finite time, t_f, corresponding to an infinite precursor rate, realization of a system-wide fracture and the percolation threshold, and often equated to the initiation of the eruption, earthquake, or landslide process (Voight, 1988).

1.1. Material failure and landslide forecasts

Theoretical considerations suggest that $\alpha \approx 2$ is typical of rock failure and landslides (Kilburn & Petley, 2003; Petley et al., 2005), in which case the inverse precursor rate is expected to decrease linearly with time to failure. This approach has been used to visualise and model the evolution in precursor (commonly ground deformation) rate, and proposed as a means to forecast the timing of future landslides (Fukozono, 1990; Kilburn & Petley, 2003; Petley, 2017c; Petley et al., 2005; Saito, 1980). However, the common practice of using least-squares regression to fit a straight line to inverse precursor rates fails to account for the complex error structure of such data, resulting in biased and inaccurate forecasts and parameter estimates (Bell, Naylor, et al., 2011). Instead, Generalized Linear Models (Bell, Naylor, et al., 2011), maximum-likelihood (Bell, Greenhough, et al., 2011) and Bayesian (Boué et al., 2015) methods have been proposed as improved methods to estimate model parameters for volcanic and laboratory data, but have yet to be applied to landslide signals. Consequently, it is not clear to what extent Equation (2) accurately models the geophysical signals preceding landslides, or the values of model parameters, including α.

The 2017 Nuugaatsiaq landslide in Greenland (Poli, 2017) highlighted the potential for small earthquakes within the landslide zone to provide precursory information about the approach to slope failure. Relatively few precursory earthquake sequences have been reported before landslides (Amitrano et al., 2005; Caplan-Auerbach & Huggel, 2007; Huggel et al., 2007; Weaver & Malone, 1979), and they are only expected for deep-seated events. Consequently, the properties of such sequences have yet to be thoroughly quantified, although theoretical considerations suggest that they may follow similar trends to ground deformation (Kilburn & Petley, 2003). In contrast, evidence from volcanic systems suggests earthquake rate and ground deformation may follow distinctly different trends in the approach to eruption (Bell & Kilburn, 2012; Kilburn, 2012). For example, before dyke intrusion events at Kilauea volcano, surface deformation was observed to follow a linear trend, whereas seismicity rates accelerated according to an exponential or power-law trend (Bell & Kilburn, 2012). Such differences may depend on whether the applied stress is increasing or constant (Kilburn, 2012; Robertson & Kilburn, 2016).

Earthquake occurrence data have different statistical properties to surface deformation data, and in general need a different modelling approach. The temporal occurrence of volcano-tectonic earthquakes and laboratory acoustic emissions is generally consistent with an inhomogeneous Poisson or clustered point process (Bell, Greenhough, et al., 2011). The source locations of such earthquakes are typically distributed throughout the medium undergoing deformation, and have a power-law distribution of sizes. In contrast, many physical systems display repeated activation of a what is likely to be a single source location in the approach to failure (Bouchon et al., 2011; Neuberg et al., 2006; Poli, 2017). Such data is characterized by a restricted range of sizes, repeating highly-similar waveforms indicating multiple reactivation of a small number of source locations (within a few hundred metres or less (Green & Neuberg, 2006)), and quasi-periodic (anti-clustered) inter-event times. Alternative statistical methods need to be consider for modelling the time evolution these data.

1.2. The 2017 Nuugaatsiaq landslide, Greenland

On the 17th June 2017, a large landslide occurred near Nuugaatsiaq, Greenland (Petley, 2017a, 2017c, 2017d; Poli, 2017). The landslide entered the sea, causing a tsunami which killed four people (Petley, 2017a, 2017b). The landslide itself generated a large seismic signal, equivalent to a magnitude 4 earthquake, and recorded at seismic stations globally (Petley, 2017a). However, in the hours before the landslide a sequence of small earthquakes were recorded at NUUG seismic station, 30km away from the landslide (Petley, 2017c, 2017d; Poli, 2017). These earthquakes showed repeating waveforms, a restricted range of amplitudes, quasi-periodic inter-event times, and a rate that increased towards the time of the landslide (Poli, 2017). Poli (2017) suggested that the earthquake rate increased according to an exponential function with time, by comparison to similar sequences recorded during the nucleation stages of large earthquakes, and Petley (2017c), suggested a linear decrease in inverse earthquake rate with time towards failure, corresponding to a hyperbolic increase in rate with time (Petley et al., 2005). However, no formal modelling of the data was undertaken in either study.

Here I apply a new Bayesian gamma point process model to analyse the repeating earthquakes preceding the June 2017 Nuugaatsiaq landslide. Earthquake rates increase over 10 hours according to the power-law form of the FFM, described by equation 2, but with quasi-periodic inter-event times. The mean posterior power-law exponent, $p = 0.71$, provides a much better fit to the data than the commonly proposed value of 1.0 (equation 4), or the exponential model proposed by Poli (2017). 'Pseudo-prospective' forecasts illustrate the potential predictability of similar landslides in future, though the rapid acceleration means that warning times are likely to be inherently short.

First I summarize the seismic data and statistical methods used. I then apply the different earthquake rate models in retrospective and simulated forecasting modes to evaluate model fit and posterior parameter distributions, and determine likely forecasting performance. I then discuss the implications of my findings for understanding of landslide processes, precursory source mechanisms, and failure forecasting.

2. Data and methods

2.1. Seismic data and catalogue generation

Seismic data for station NUUG for 17th June 2017 was accessed through the Incorporated Research Institutions for Seismology (IRIS), and manipulated using the Obspy python library (Krischer et al., 2015). Following initial data inspection and bandpass filtering between 2 and 20Hz an initial catalogue was picked from the HHZ component using a standard STA/LTA algorithm. As reported by Poli (2017), earthquakes in this initial catalogue have similar waveforms (indicating closely co-located sources), and locally quasi-periodic inter-event times. Following the method of Poli (2017), a cross-correlation template-matching approach was employed to identify other similar waveforms not picked using the STA/LTA method. All earthquakes in the initial catalogue were cross-correlated with each other. The most highly co-correlated waveform in the initial catalogue was used as the template waveform. This earthquake occurred at 23:27:33 on 17th June. The size of the resulting catalogue is dependent on the final cross-correlation threshold used to define an earthquake occurrence (and dependent on factors such as waveform length and filtering). The preferred catalogue, using a cross-correlation value of 0.3 and an earthquake duration of 10 s, contains 89 earthquakes (compared to 95 in Poli (2017)). The cross-correlation time-series, threshold, and

pick times are shown in supplemental Fig. 1. All 89 earthquakes within this catalogue occurred between 14:41:33 and 23:39:05 on 17th June. Modelling and forecasting analyses are relatively insensitive to small changes in the catalogue resulting from a slightly different choice of cross-correlation threshold within realistic bounds. A threshold of 0.275 returns 92 earthquakes, and one of 0.325 returns 87 earthquakes. I define the onset of the landslide process as the arrival of high amplitude seismic waves at NUUG at 23:39:20, with an uncertainty of about 30 seconds.

2.2. Periodicity

I define periodicity as the ratio between the mean and standard deviation of the inter-event times (Bell et al., 2017). For a constant average earthquake rate, λ, for earthquakes that are randomly distributed in time (i.e. a Poisson process), the inter-event times follow an exponential distribution with mean $\mu = 1/\lambda$ and variance $\sigma^2 = 1/\lambda^2$. Therefore, the periodicity, $\mu/\sigma = 1$. The variance of inter-event times for earthquakes that are clustered in time (such as typical tectonic earthquakes), will be relatively high, giving values of periodicity less than 1. The variance of highly periodic (anti-clustered) earthquakes will be relatively small, resulting in periodicity values greater than 1. For highly-periodic volcanic 'drumbeat' earthquakes, periodicity values of up to 6 have been reported (Bell et al., 2017). For data with a systematically changing average earthquake rate, the inter-event time distribution and periodicity need to be determined once this trend has been accounted for.

2.3. Gamma point process models and Bayesian parameter estimation

Quasi-periodic earthquake occurrence time data, such as this precursory sequence, have different statistical properties to random or clustered times. Consequently, in order to accurately model the evolving underlying occurrence rate of such data, it is necessary to consider alternative approaches to the commonly used least-squares regression to inverse rate data or Poisson maximum-likelihood methods. Here, I consider earthquake times as a point process, where earthquakes occur as 'spikes' on timeline, defined by both a time-varying mean rate of occurrence and the nature of the spacing between consecutive spikes.

Specifically, I model quasi-periodic inter-event times as an inhomogeneous gamma point process (Barbieri et al., 2001), with a mean rate evolving according to Equations (2)-(4). This approach allows the estimation of the parameters of the underlying rate model, but accounting for consecutive occurrence times that are 'anti-clustered', i.e. after an earthquake happens the probability of a subsequent earthquake is less than that if their occurrence was random in time. One such inter-event time distribution is the gamma distribution, and hence a gamma process is a generalized form of Poisson process for quasi-periodic data where inter-event times follow a gamma distribution. A Gamma process has been used to analyse quasi-periodic biomedical data, such as neuron spiking (Barbieri et al., 2001) and heartbeats (Barbieri et al., 2005).

I use a Markov Chain Monte Carlo method (MCMC) to estimate model parameter posterior distributions, efficiently evaluating the log likelihood function of the inhomogeneous gamma point process (see Supplemental Text) for many parameter combinations, implemented through PyMC3 (Salvatier et al., 2016). This Bayesian approach allows consideration of a realistic set of model parameter values through incorporation of prior distributions (Boué et al., 2015), and describing the probability of parameter values given the data and prior belief as a posterior distribution. These distributions can be characterized by a mean or mode and a highest posterior density interval (the narrowest range of parameter values within which there is a given probability of the true value lying).

3. Results

3.1. Precursors to failure

Average earthquake rates increased systematically in the 12 hr lead up to the 17 June landslide. Continuous waveform data shows distinct discrete earthquakes above the background noise (Fig. 1). Earthquake amplitudes have a restricted range of values (they are not consistent with a Gutenberg-Richter distribution). They generally increase through the precursory sequence, before decreasing slightly 10 minutes before failure. A final increase in amplitudes immediately before failure is likely to result from overlap of closely spaced earthquakes (Fig. 1d). Inter-event times are evidently quasi-periodic, and systematically decrease with time towards failure from greater than 1000 s to less than 10 s close to failure.

3.2. Retrospective modelling of precursory earthquake time-series

The catalogue of earthquake times preceding the landslide were modelled as an inhomogeneous gamma point process, with average rate evolving according to equations (2)-(4). Firstly, this was undertaken as a 'retrospective' analysis, where the failure time is known, and fixed. Example results of this analysis are shown in Fig (2). The left hand panels show hourly earthquake rate and total number of earthquakes as a function of time. The central panels show the inverse inter-event time and hourly earthquake rate as a function of time before failure on log-log axes. In this space, a power-law acceleration in rate (equation (2)) will take the form of a straight line, with slope $-p$. The right hand panels show inverse inter-event time and hourly earthquake rate as a function of time before failure on linear-log axes. In this space, an exponential increase in rate with time (equation (3)) will take the form of a straight line with slope $-\lambda$. In each case, the red lines represent 500 samples from the posterior parameter distributions for the power-law (top row), hyperbolic (middle row), and exponential models (bottom row).

The power-law model with mean posterior value of $p = 0.71$ clearly provides an excellent fit to the data, and explains its evolution better than either the hyperbolic or exponential models. The 95% highest posterior density interval (HPDI) for p is [0.67, 0.74]. The hyperbolic model systematically underestimates early rates and overestimates later rates, and the exponential model is unable to explain the rapid acceleration in rate as failure is approached. The scatter in inter-event times around the general trend is small, and is particularly apparent in log-log space. This feature reflects the highly periodic nature of the earthquake process; a Poisson process would involve a much greater scatter in inter-event times. For all models, the periodicity is high; for the power-law model, aggregated over the full dataset its value is 5.8, comparable to the highest values observed for volcanic drumbeat earthquakes (Bell et al., 2017).

3.3. Pseudo-prospective forecasts and temporal evolution of posterior parameter distributions

Repeated 'pseudo-prospective' forecasts, where the failure time is unknown, and data is added incrementally as if it were becoming available in real-time, reveal the evolution of parameter posterior distributions as the sequence progresses, and provide insights in to the potential for using repeating earthquakes for forecasting the timing of similar landslides in future as part of an operational decision making process for risk reduction. Figure 3 illustrates the evolution of the posterior probability distributions for the forecast failure time, p, and periodicity for the power-law model (equation (2)) for the second half of the precursory sequence. Until 90% of the sequence is complete, few earthquakes have occurred, there is

little information on which to estimate parameter values, and the posterior distributions are strongly influenced by the priors. The mean of the log-normal prior distribution for p is higher than the true value, and so the parameter covariance means that the mean of the posterior for the forecast failure time is slightly late, though the true value is within the 90% credible interval. As the earthquake rate increases after 90% of the sequence is complete, more information becomes available and the posterior distributions quickly converge on the retrospectively determined values. At 96% of the sequence completed (22 minutes before failure), the 95% HPDIs for the failure time are [-16 mins, +12 mins]. If one were to know the true value of $p = 0.71$ in advance, the posterior distributions converge on the true values much earlier in the sequence (Figure 4), and the uncertainty in the forecast time would be significantly reduced. The corresponding 95% HPDIs for the failure time at 96% of the sequence completed are [-8 mins, +4 mins].

4. Discussion

The earthquake sequence preceding failure was characterized by highly-similar earthquake waveforms, locally periodic inter-event times, and a restricted range of amplitudes. These characteristics are not consistent with seismicity directly resulting from distributed fracturing within a deforming rock mass. Instead, they require either re-activation of a single localized asperity, which repeatedly fails and heals, or perhaps progressive failure of a series of closely co-located asperities. Continued loading is driven by otherwise aseismic accelerating slip along a larger (and perhaps growing) fault surface, as suggested by Poli (2017). Short inter-event times close to the failure time imply that rapid (<10 s) healing, loading, and failure of the earthquake source was possible, possibly suggesting mechanical healing through interlocking.

Petley *et al.* (2002) argue from a theoretical and empirical basis that two forms of precursory acceleration exist. For a crack nucleation process, the acceleration should follow an exponential trend, and for a crack growth process, it should follow a hyperbolic trend with $p = 1$. Shallow landslides are expected to behave in a non-brittle manner, with exponential trends, so this model is unlikely to be appropriate for the deep-seated Nuugaatsiaq landslide. In addition to providing a poor fit to the data, an exponential model does not define a finite failure time (Bell, Greenhough, et al., 2011), and so failure time forecasts using this approach are likely to be significantly more inaccurate than the preferred power-law model.

The modelling here indicates that the acceleration in average earthquake rate is best explained by a systematic power-law increase with time, with a power-law exponent $p = 0.71$ and within the range of 0.67 to 0.74 to 95% probability. This parameter value represents a rapid, more non-linear acceleration than the hyperbolic trend. In the context of the inverse rate analyses by Petley *et al.* (2002), this corresponds to a concave function in $\Lambda - \mathrm{t}$ space, where $\Lambda = 1/\lambda(t)$, rather than the asymptotic (convex) function expected for crack nucleation or linear function for crack growth. Amitrano *et al*. (2005) find a value of $p = 0.87 \pm 0.06$ for seismicity rates before a cliff failure. Values of $p < 1$ are commonly reported for potentially analogous earthquake foreshock sequences (Peng et al., 2007), and observed for simulations based on by frictional sliding laws (Dieterich & Kilgore, 1996; Ziv, 2003) and epidemic-type models (Helmstetter et al., 2003). Although it is impossible to exclude a more complex model (such as an exponential acceleration evolving in to a power-law acceleration), this additional complexity is not required to explain the data.

A rapidly accelerating sequence like this means that a small proportion of earthquakes occur in the early part of the sequence, and thus the inherent predictability is less than for a slower acceleration. Consequently, if all precursory earthquake sequences to landslides behave in this manner, one should expect relatively short warning times based on seismicity

alone, even for highly periodic data. Ground deformation and local seismic monitoring data may have been able to identify additional precursory signals over a longer period of time, perhaps including an initiation phase. In practice, if sufficiently good data processing and earthquake identification methods had been in operation, early warning of a possible landslide could have been issued from these data alone by about 18:00, when repeating earthquakes and an accelerating trend become apparent. At this point the modelling approach described here could have been employed to quantify the evolving trend, check its progression, and issue probabilistic forecasts of landslide timing. The final onset of the landslide itself, and generation of the subsequent tsunami happened within a few minutes, providing little opportunity for action.

5. Conclusions

This work outlines a new approach for reliable and informative retrospective analyses of pre-failure seismicity, and verifiable and testable Bayesian forecasts of landslide failure times. The precursory seismicity before the June 2017 Nuugaatsiaq landslide is closely approximated by an inhomogeneous gamma point-process, with a power-law acceleration in average earthquake rate, and strongly periodic inter-event times. The mean posterior power-law exponent of $p = 0.71$ is lower than that predicted by material failure models for landslide occurrence. As the predictive power of forecasting methods depends on our prior knowledge of model parameters, further empirical and theoretical work is required to quantify and understand these for different geophysical signals and in a range of material failure systems.

Acknowledgments

Data used is this study are openly available from through IRIS. I thank Chris Kilburn, Al Handwerger, Simon Mudd, and Ian Main for helpful discussions. I also thank Jackie Caplan-Auerbach and an anonymous reviewer for their constructive comments that helped improve the manuscript.

References

Amitrano, D., Grasso, J. R., & Senfaute, G. (2005). Seismic precursory patterns before a cliff collapse and critical point phenomena. *Geophysical Research Letters*, *32*(8), L08314. https://doi.org/10.1029/2004GL022270

Barbieri, R., Quirk, M. C., Frank, L. M., Wilson, M. A., & Brown, E. N. (2001). Construction and analysis of non-Poisson stimulus-response models of neural spiking activity. *Journal of Neuroscience Methods*, *105*(1), 25–37. https://doi.org/10.1016/S0165-0270(00)00344-7

Barbieri, R., Matten, E. C., Alabi, A. a, & Brown, E. N. (2005). A point-process model of human heartbeat intervals: new de nitions of heart rate and heart rate variability. *Am J Physiol Heart Circ Physiol*, *288*, 424–435. https://doi.org/10.1152/ajpheart.00482.2003.A

Bell, A. F., Hernandez, S., Gaunt, H. E., Mothes, P. A., Ruiz, M., Sierra, D., & Aguaiza, S. (2017). The rise and fall of periodic "drumbeat" seismicity at Tungurahua volcano, Ecuador. *Earth and Planetary Science Letters*, *475*, 58–70. https://doi.org/10.1016/j.epsl.2017.07.030

Bell, A. F., & Kilburn, C. R. J. (2012). Precursors to dyke-fed eruptions at basaltic volcanoes: Insights from patterns of volcano-tectonic seismicity at Kilauea volcano, Hawaii. *Bulletin of Volcanology*, *74*(2), 325–339. https://doi.org/10.1007/s00445-011-0519-3

Bell, A. F., & Kilburn, C. R. J. (2013). Trends in the aggregated rate of pre-eruptive volcano-tectonic seismicity at Kilauea volcano, Hawaii. *Bulletin of Volcanology*, *75*(1), 1–10. https://doi.org/10.1007/s00445-012-0677-y

Bell, A. F., Greenhough, J., Heap, M. J., & Main, I. G. (2011). Challenges for forecasting based on accelerating rates of earthquakes at volcanoes and laboratory analogues. *Geophysical Journal International*, *185*(2), 718–723. https://doi.org/10.1111/j.1365-246X.2011.04982.x

Bell, A. F., Naylor, M., Heap, M. J., & Main, I. G. (2011). Forecasting volcanic eruptions and other material failure phenomena: An evaluation of the failure forecast method. *Geophysical Research Letters*, *38*(15), n/a-n/a. https://doi.org/10.1029/2011GL048155

Bouchon, M., Karabulut, H., Aktar, M., Ozalaybey, S., Schmittbuhl, J., & Bouin, M.-P. (2011). Extended Nucleation of the 1999 Mw 7.6 Izmit Earthquake. *Science*, *331*(6019), 877–880. https://doi.org/10.1126/science.1197341

Boué, A., Lesage, P., Cortés, G., Valette, B., & Reyes-Dávila, G. (2015). Real-time eruption forecasting using the material Failure Forecast Method with a Bayesian approach. *Journal of Geophysical Research: Solid Earth*, *120*(4), 2143–2161. https://doi.org/10.1002/2014JB011637

Caplan-Auerbach, J., & Huggel, C. (2007). Precursory seismicity associated with frequent, large ice avalanches on Iliamna volcano, Alaska, USA. *Journal of Glaciology*, *53*(180), 128–140. https://doi.org/10.3189/172756507781833866

Dieterich, J. H., & Kilgore, B. (1996). Implications of fault constitutive properties for earthquake prediction. *Proceedings of the National Academy of Sciences*, *93*(9), 3787–3794. https://doi.org/10.1073/pnas.93.9.3787

Dmitrieva, K., Hotovec-Ellis, A. J., Prejean, S. G., & Dunham, E. M. (2013). Frictional-faulting model for harmonic tremor before Redoubt Volcano eruptions. *Nature Geoscience*, *6*(8), 652–656. https://doi.org/10.1038/ngeo1879

Fukozono, T. (1990). Recent studies on time prediction of slope failure. *Landslide News*, *4*, 9–12.

Green, D. N., & Neuberg, J. (2006). Waveform classification of volcanic low-frequency

373 earthquake swarms and its implication at Soufrière Hills Volcano, Montserrat. *Journal*
374 *of Volcanology and Geothermal Research*, *153*(1–2), 51–63.
375 https://doi.org/10.1016/j.jvolgeores.2005.08.003
376 Helmstetter, A., Sornette, D., & Grasso, J.-R. (2003). Mainshocks are aftershocks of
377 conditional foreshocks: How do foreshock statistical properties emerge from aftershock
378 laws. *Journal of Geophysical Research: Solid Earth*, *108*(B1), 1–24.
379 https://doi.org/10.1029/2002JB001991
380 Huggel, C., Gruber, S., Caplan-Auerbach, J., Wessels, R. L., & Molnia, B. F. (2007). The
381 2005 Mt. Steller, Alaska, rock-ice avalanche: What does it tell us about large slope
382 failures in cold permafrost? *Analysis*, (Osterkamp), 747–752.
383 https://doi.org/10.5167/uzh-3097
384 Intrieri, E., Raspini, F., Fumagalli, A., Lu, P., Del Conte, S., Farina, P., … Casagli, N. (2017).
385 The Maoxian landslide as seen from space: detecting precursors of failure with Sentinel-
386 1 data. *Landslides*, (October), 1–11. https://doi.org/10.1007/s10346-017-0915-7
387 Kilburn, C. R. J. (2003). Multiscale fracturing as a key to forecasting volcanic eruptions.
388 *Journal of Volcanology and Geothermal Research*, *125*(3–4), 271–289.
389 https://doi.org/10.1016/S0377-0273(03)00117-3
390 Kilburn, C. R. J. (2012). Precursory deformation and fracture before brittle rock failure and
391 potential application to volcanic unrest. *Journal of Geophysical Research: Solid Earth*,
392 *117*(B2), n/a-n/a. https://doi.org/10.1029/2011JB008703
393 Kilburn, C. R. J., & Petley, D. N. (2003). Forecasting giant, catastrophic slope collapse:
394 lessons from Vajont, Northern Italy. *Geomorphology*, *54*(1–2), 21–32.
395 https://doi.org/10.1016/S0169-555X(03)00052-7
396 Krischer, L., Megies, T., Barsch, R., Beyreuther, M., Lecocq, T., Caudron, C., &
397 Wassermann, J. (2015). ObsPy: a bridge for seismology into the scientific Python
398 ecosystem. *Computational Science & Discovery*, *8*(1), 14003.
399 https://doi.org/10.1088/1749-4699/8/1/014003
400 De La Cruz-Reyna, S., & Reyes-Dávila, G. A. (2001). A model to describe precursory
401 material-failure phenomena: Applications to short-term forecasting at Colima volcano,
402 Mexico. *Bulletin of Volcanology*, *63*(5), 297–308.
403 https://doi.org/10.1007/s004450100152
404 Main, I. G. (1999). Applicability of time-to-failure analysis to accelerated strain before
405 earthquakes and volcanic eruptions. *Geophysical Journal International*, *139*(3), F1–F6.
406 https://doi.org/10.1046/j.1365-246x.1999.00004.x
407 Minakami T. (1960). Fundamental Research for Predicting Volcanic Eruptions. Part 1.
408 *Bulletin of the Earthquake Research Institute*, *47*(Seismometrical Surveys of Volcanoes
409 in Japana and Volcano Sotara in Colombia), 893–949.
410 Neuberg, J., Tuffen, H., Collier, L., Green, D., Powell, T., & Dingwell, D. (2006). The trigger
411 mechanism of low-frequency earthquakes on Montserrat. *Journal of Volcanology and*
412 *Geothermal Research*, *153*(1–2), 37–50.
413 https://doi.org/10.1016/j.jvolgeores.2005.08.008
414 Omori, F. (1916). The Sakura-Jima eruptions and earthquakes. V. - 1920. *Bulletin of the*
415 *Volcanological Society of Japan*, *8*(2), 35–179.
416 Peng, Z., Vidale, J. E., Ishii, M., & Helmstetter, A. (2007). Seismicity rate immediately
417 before and after main shock rupture from high-frequency waveforms in Japan. *Journal*
418 *of Geophysical Research*, *112*(B3), B03306. https://doi.org/10.1029/2006JB004386
419 Petley, D. N. (2017a). Much more detail about the Greenland landslide and tsunami,
420 including images and video [Blog post]. Retrieved December 5, 2017, from
421 https://blogs.agu.org/landslideblog/2017/06/21/greenland-landslide-3/
422 Petley, D. N. (2017b). Nuugaatsiaq: A large landslide-induced tsunami on Saturday night?

[Blog post]. Retrieved December 5, 2017, from https://blogs.agu.org/landslideblog/2017/06/19/nuugaatsiaq/

Petley, D. N. (2017c). The Nuugaatsiaq landslide in Greenland: understanding the failure processes [Blog post]. Retrieved December 5, 2017, from https://blogs.agu.org/landslideblog/2017/11/06/nuugaatsiaq-landslide/

Petley, D. N. (2017d). Updates from the Karrat Fjord landslide in Greenland [Blog post]. Retrieved December 5, 2017, from https://blogs.agu.org/landslideblog/2017/08/08/karrat-fjord-landslide/

Petley, D. N., Higuchi, T., Petley, D. J., Bulmer, M. H., & Carey, J. (2005). Development of progressive landslide failure in cohesive materials. *Geology*, *33*(3), 201. https://doi.org/10.1130/G21147.1

Petley, D. N., Bulmer, M. H., & Murphy, W. (2002). Patterns of movement in rotational and translational landslides. *Geology*, *30*(8), 719. https://doi.org/10.1130/0091-7613(2002)030<0719:POMIRA>2.0.CO;2

Poli, P. (2017). Creep and slip: Seismic precursors to the Nuugaatsiaq landslide (Greenland). *Geophysical Research Letters*, *44*(17), 8832–8836. https://doi.org/10.1002/2017GL075039

Robertson, R. M., & Kilburn, C. R. J. (2016). Deformation regime and long-term precursors to eruption at large calderas: Rabaul, Papua New Guinea. *Earth and Planetary Science Letters*, *438*(September 1994), 86–94. https://doi.org/10.1016/j.epsl.2016.01.003

Saito, M. (1980). Semi-logarithmic representation for forecasting slope failure. In *International Symposium on Landslides* (Vol. 1, pp. 321–324). Meerut, India: Sarita Prakashan.

Salvage, R. O., & Neuberg, J. (2016). Using a cross correlation technique to refine the accuracy of the Failure Forecast Method: Application to Soufrière Hills volcano, Montserrat. *Journal of Volcanology and Geothermal Research*, *324*, 118–133. https://doi.org/10.1016/j.jvolgeores.2016.05.011

Salvatier, J., Wiecki, T. V., & Fonnesbeck, C. (2016). Probabilistic programming in Python using PyMC3. *PeerJ Computer Science*, *2*, e55. https://doi.org/10.7717/peerj-cs.55

Tokarev, P. I. (1963). On a possibility of forecasting of bezymianny volcano eruptions according to seismic data. *Bulletin Volcanologique*, *26*(1), 379–386. https://doi.org/10.1007/BF02597299

Vasseur, J., Wadsworth, F. B., Heap, M. J., Main, I. G., Lavallée, Y., & Dingwell, D. B. (2017). Does an inter-flaw length control the accuracy of rupture forecasting in geological materials? *Earth and Planetary Science Letters*, *475*(August), 181–189. https://doi.org/10.1016/j.epsl.2017.07.011

Voight, B. (1988). A method for prediction of volcanic eruptions. *Nature*, *332*(6160), 125–130. https://doi.org/10.1038/332125a0

Weaver, C. S., & Malone, S. D. (1979). Seismic Evidence for Discrete Glacier Motion at the Rock–Ice Interface. *Journal of Glaciology*, *23*(89), 171–184. https://doi.org/10.1017/S0022143000029816

Ziv, A. (2003). Foreshocks, aftershocks, and remote triggering in quasi-static fault models. *Journal of Geophysical Research: Solid Earth*, *108*(B10), 1–13. https://doi.org/10.1029/2002JB002318

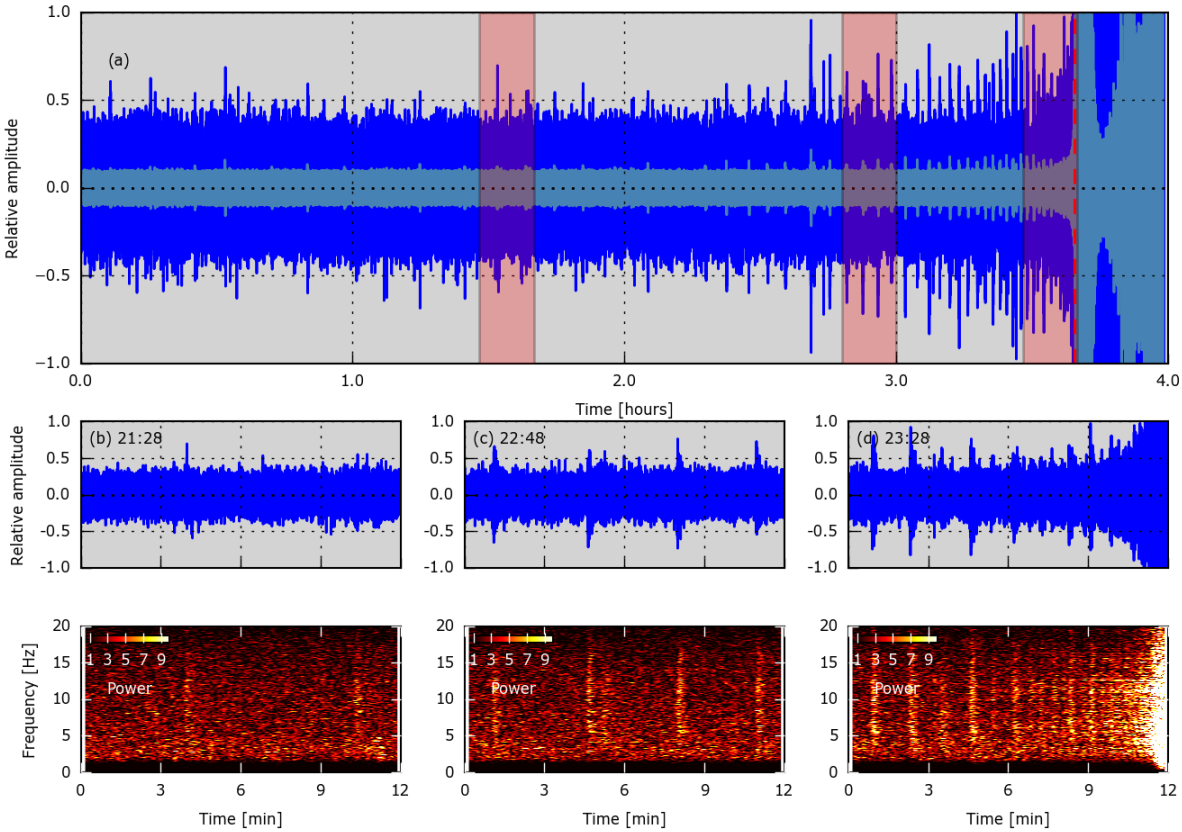

Figure 1: (a) Velocity time series for four hours of data recorded on channel HHZ at NUUG between 20:00 and 24:00 UTC on 17th June 2017, documenting the increase in earthquake rate before landslide failure at 23:39 (dashed red line). Dark blue line represents data bandpass filtered between 2 Hz and 20 Hz; light blue line represents 10 second average amplitude. (b)-(d) 12 minute times series and relative power spectrograms for the intervals indicated by red bars in (a), and starting at 21:28, 22:48, and 23:28, respectively. Precursory earthquakes appear as transient signals above the background noise.

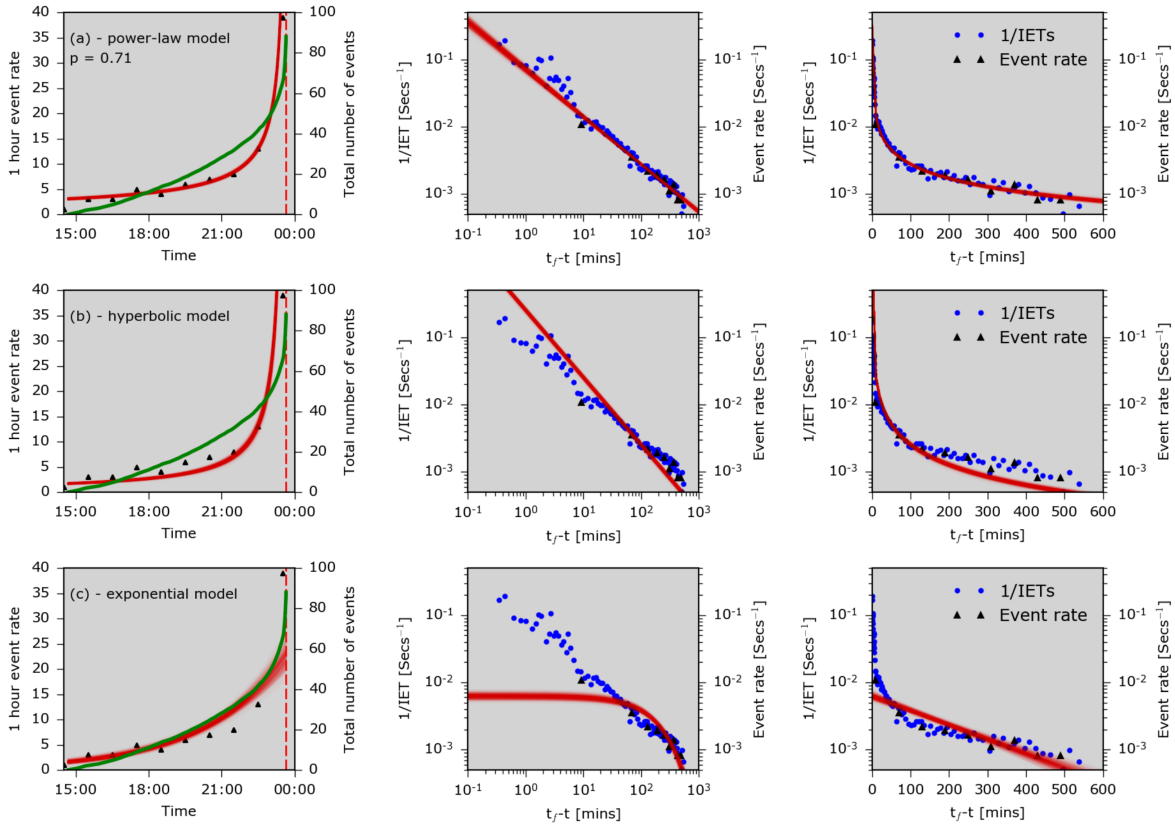

Figure 2: Linear time (left panels), log-log time from failure (centre panels), and linear-log time from failure (right panels) plots for (a) power-law model, (b) hyperbolic model, and (c) exponential model. In left panels, green line represents total number of earthquakes as a function of time. Black triangles represent hourly earthquake rates, and blue circles represent the inverse inter-event time ('1/IET', or local earthquake rate). Red lines represent a superposition of 500 MCMC samples from 'retrospective' posterior parameter distributions, with known failure time.

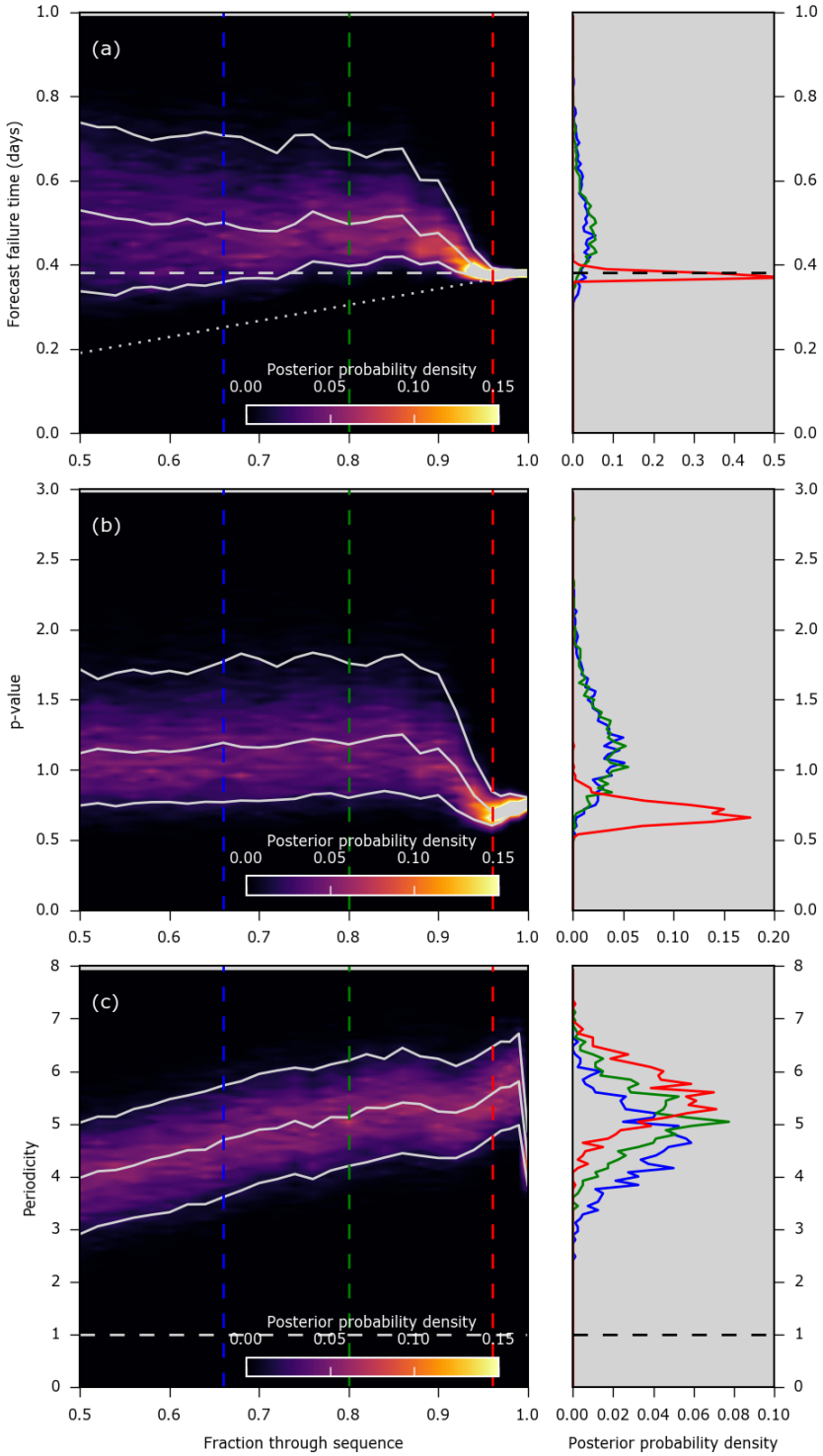

Figure 3: Left panels: Evolution of posterior distribution of (a) failure time; (b) p; and (c) periodicity (horizontal dashed line representing a homogeneous Poisson process for reference), based on earthquake occurrence times for power-law average rate model. Colour scale indicateds the posterior probability density for parameters. White lines indicate the mean and 5% and 95% credibility intervals of the posterior. In (a), horizontal white dashed line indicates true value of landslide time, and dotted white line indicates actual time at which hindcast is made. Right panel: Posterior probability density functions at times indicated by correspondingly coloured dashed lines in left panel (at fractions of 0.66, 0.8, and 0.96 of the sequence).

496

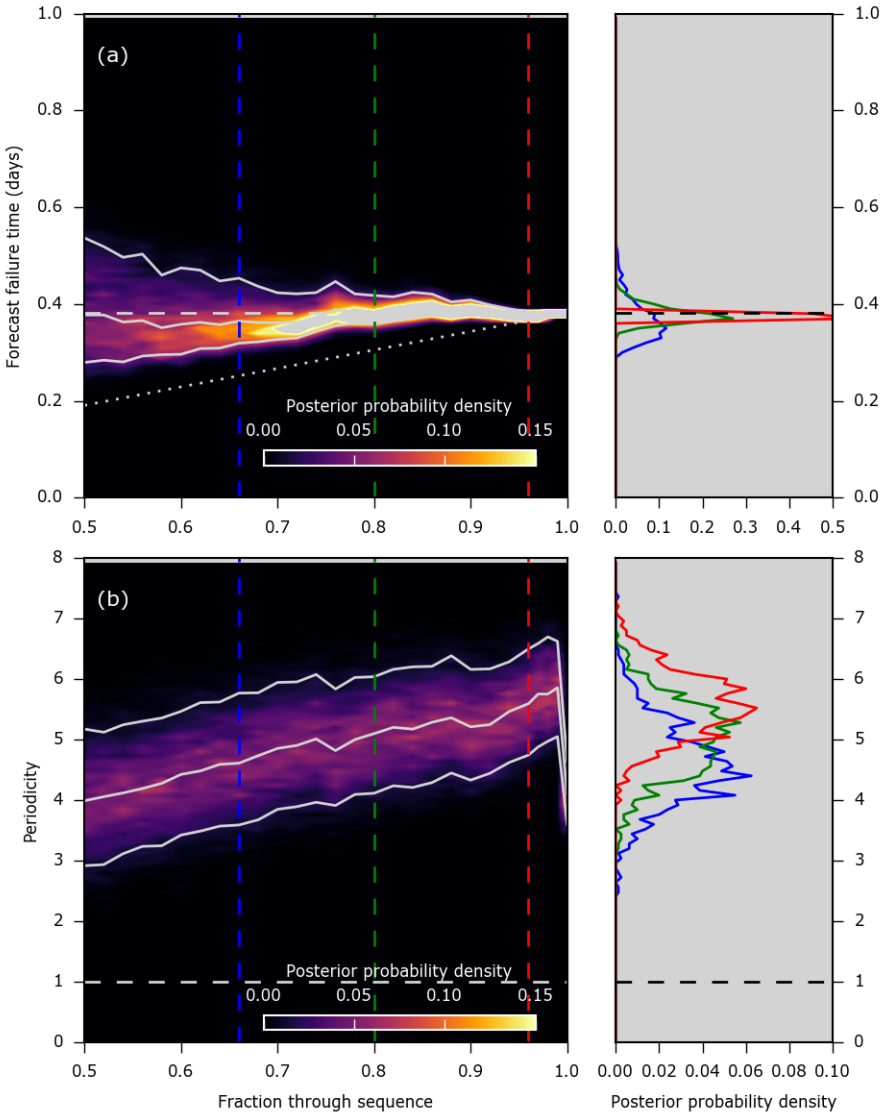

497

498 **Figure 4**: Figure as for Figure 3, but for power-law model wth fixed $p = 0.71$. Note rapid
499 convergence of posterior distribution of failure time on true value.